Study of the Hadronic Decays of χ_c States

J. Z. Bai,[1] Y. Ban,[5] J. G. Bian,[1] I. Blum,[12] G. P. Chen,[1] H. F. Chen,[11] J. Chen,[3] J. C. Chen,[1] Y. Chen,[1] Y. B. Chen,[1] Y. Q. Chen,[1] B. S. Cheng,[1] X. Z. Cui,[1] H. L. Ding,[1] L. Y. Dong,[1] Z. Z. Du,[1] W. Dunwoodie,[8] C. S. Gao,[1] M. L. Gao,[1] S. Q. Gao,[1] P. Gratton,[12] J. H. Gu,[1] S. D. Gu,[1] W. X. Gu,[1] Y. F. Gu,[1] Y. N. Guo,[1] S. W. Han,[1] Y. Han,[1] F. A. Harris,[9] J. He,[1] J. T. He,[1] K. L. He,[1] M. He,[6] D. G. Hitlin,[2] G. Y. Hu,[1] H. M. Hu,[1] J. L. Hu,[1] Q. H. Hu,[1] T. Hu,[1] X. Q. Hu,[1] Y. Z. Huang,[1] J. M. Izen[12], C. H. Jiang,[1] Y. Jin,[1] B. D. Jones,[12] Z. J. Ke[1], M. H. Kelsey,[2] B. K. Kim,[12] D. Kong,[9] Y. F. Lai,[1] P. F. Lang,[1] A. Lankford,[10] C. G. Li,[1] D. Li,[1] H. B. Li,[1] J. Li,[1] P. Q. Li,[1] R. B. Li,[1] W. Li,[1] W. G. Li,[1] X. H. Li,[1] X. N. Li,[1] H. M. Liu,[1] J. Liu,[1] R. G. Liu,[1] Y. Liu,[1] X. C. Lou,[12] B. Lowery,[12] F. Lu,[1] J. G. Lu,[1] X. L. Luo,[1] E. C. Ma,[1] J. M. Ma,[1] R. Malchow,[3] H. S. Mao,[1] Z. P. Mao,[1] X. C. Meng,[1] J. Nie,[1] S. L. Olsen,[9] J. Oyang,[2] D. Paluselli,[9] L. J. Pan,[9] J. Panetta,[2] F. Porter,[2] N. D. Qi,[1] X. R. Qi,[1] C. D. Qian,[7] J. F. Qiu,[1] Y. H. Qu,[1] Y. K. Que,[1] G. Rong,[1] M. Schernau,[10] Y. Y. Shao,[1] B. W. Shen,[1] D. L. Shen,[1] H. Shen,[1] X. Y. Shen,[1] H. Y. Sheng,[1] H. Z. Shi,[1] X. F. Song,[1] J. Standifird,[12] F. Sun,[1] H. S. Sun,[1] Y. Sun,[1] Y. Z. Sun,[1] S. Q. Tang,[1] W. Toki,[3] G. L. Tong,[1] G. S. Varner,[9] F. Wang,[1] L. S. Wang,[1] L. Z. Wang,[1] Meng Wang,[1] P. Wang,[1] P. L. Wang[1], S. M. Wang,[1] T. J. Wang,[1†] Y. Y. Wang,[1] M. Weaver,[2] C. L. Wei,[1] Y. G. Wu,[1] D. M. Xi,[1] X. M. Xia,[1] P. P. Xie,[1] Y. Xie,[1] Y. H. Xie,[1] G. F. Xu,[1] S. T. Xue,[1] J. Yan,[1] W. G. Yan,[1] C. M. Yang,[1] C. Y. Yang,[1] J. Yang,[1] W. Yang,[3] X. F. Yang,[1] M. H. Ye,[1] S. W. Ye,[11] Y. X. Ye,[11] C. S. Yu,[1] C. X. Yu,[1] G. W. Yu,[1] Y. H. Yu,[4] Z. Q. Yu,[1] C. Z. Yuan,[1] Y. Yuan,[1] B. Y. Zhang,[1] C. C. Zhang,[1] D. H. Zhang,[1] Dehong zhang,[1] H. L. Zhang,[1] J. Zhang,[1] J. W. Zhang,[1] L. S. Zhang,[1] Q. J. Zhang,[1] S. Q. Zhang,[1] X. Y. Zhang,[6] Y. Y. Zhang,[1] D. X. Zhao,[1] H. W. Zhao,[1] Jiawei Zhao,[11] J. W. Zhao,[1] M. Zhao,[1] W. R. Zhao,[1] Z. G. Zhao,[1] J. P. Zheng,[1] L. S. Zheng,[1] Z. P. Zheng,[1] B. Q. Zhou,[1] G. P. Zhou,[1] H. S. Zhou,[1] L. Zhou,[1] K. J. Zhu,[1] Q. M. Zhu,[1] Y. C. Zhu,[1] Y. S. Zhu,[1] and B. A. Zhuang[1]

(BES Collaboration)

[1] *Institute of High Energy Physics, Beijing 100039, People's Republic of China*

[2] *California Institute of Technology, Pasadena, California 91125*

[3] *Colorado State University, Fort Collins, Colorado 80523*

[4] *Hangzhou University, Hangzhou 310028, People's Republic of China*

[5] *Peking University, Beijing 100871, People's Republic of China*

[6] *Shandong University, Jinan 250100, People's Republic of China*

[7] *Shanghai Jiaotong University, Shanghai 200030, People's Republic of China*

[8] *Stanford Linear Accelerator Center, Stanford, California 94309*

[9] *University of Hawaii, Honolulu, Hawaii 96822*

[10] *University of California at Irvine, Irvine, California 92717*

[11] *University of Science and Technology of China, Hefei 230026, People's Republic of China*

[12] *University of Texas at Dallas, Richardson, Texas 75083-0688*

(November 5, 1998)

Abstract

Hadronic decays of the P-wave spin-triplet charmonium states $\chi_{cJ}(J = 0,1,2)$ are studied using a sample of $\psi(2S)$ decays collected by the BES detector operating at the BEPC storage ring. Branching fractions for the decays $\chi_{c1} \to K^0_s K^+\pi^- + c.c.$, $\chi_{c0} \to K^0_s K^0_s$, $\chi_{c2} \to K^0_s K^0_s$, $\chi_{c0} \to \phi\phi$, $\chi_{c2} \to \phi\phi$ and $\chi_{cJ} \to K^+K^-K^+K^-$ are measured for the first time and those for $\chi_{cJ} \to \pi^+\pi^-\pi^+\pi^-$, $\chi_{cJ} \to \pi^+\pi^-K^+K^-$, $\chi_{cJ} \to \pi^+\pi^-p\bar{p}$ and $\chi_{cJ} \to 3(\pi^+\pi^-)$ are measured with improved precision. In addition, we determine the masses of the χ_{c0} and η_c to be $M_{\chi_{c0}} = 3414.1 \pm 0.6(stat) \pm 0.8(sys)$ MeV and $M_{\eta_c} = 2975.8 \pm 3.9(stat) \pm 1.2(sys)$ MeV.

PACS numbers: 13.25.Gv, 14.40.Gx

Typeset using REVTEX

I. INTRODUCTION

The P-wave spin-triplet charmonium states were originally observed [1] in radiative decays of the $\psi(2S)$ soon after the discovery of the J/ψ and $\psi(2S)$ resonances. A number of decay modes of these states have been observed and branching fractions reported [2]. Most of the existing results are from the Mark-1 experiment, which had a data sample of 0.33 million $\psi(2S)$ decays [3]. Because the photon capabilities of the Mark-1 detector were limited, the detection of the photon from the $\psi(2S) \to \gamma\chi_{cJ}$ process was not required, and one-constraint (1C) kinematic fit was used to reconstruct the final states.

Recently there has been a renewed interest in the P-wave charmonium states. In the lowest order of perturbative QCD, the χ_{c0} and χ_{c2} decay via annihilation into two gluons while the χ_{c1} decays via $q\bar{q}g$. Information about gluon dynamics can be obtained by studying the systematics of the χ_{cJ} hadronic decays. Since the χ_{c0} and χ_{c2} mesons decay by the annihilation of the $c\bar{c}$ pair into two gluons, followed by the hadronization of the two gluons into light mesons (baryons), the latter is similar to the decay of a bound gg state; a detailed knowledge of the hadronic decays of the χ_{cJ} will provide a deeper understanding of the glueball decay patterns that may help in their identification.

The mass differences between the three χ_c states provide information on the spin-orbit and tensor interactions in non-relativistic potential models and lattics QCD calculations. The masses of the χ_{c1} and χ_{c2} have been precisely determined (to a level of $\sim \pm 0.12$ MeV) by Fermilab experiment E760 [4] using the line shape measured in the $p\bar{p} \to \chi_{c1,2}$ formation reaction. In contrast, the χ_{c0} mass is much more poorly known; the PDG average for $M_{\chi_{c0}}$ has an uncertainty of ± 2.8 MeV [2].

In this paper, we report the analyses of all-charged-track final states from χ_{cJ} decays, including $\pi^+\pi^-\pi^+\pi^-$, $\pi^+\pi^-K^+K^-$, $\pi^+\pi^-p\bar{p}$, $K^+K^-K^+K^-$, $K^0_sK^+\pi^- + c.c.$ and $3(\pi^+\pi^-)$. The results for χ_{cJ} decays into $\pi^+\pi^-$, K^+K^- and $p\bar{p}$ have been reported elsewhere [5]. We use the combined invariant mass distribution from all of the channels under study to determine the χ_{c0} mass with improved precision.

As a byproduct of this analysis, we determine the mass of the η_c. This is of interest because the $M_{J/\psi} - M_{\eta_c}$ mass difference measures the strength of the hyperfine splitting term in heavy quark interactions. However, in spite of a number of measurements, the current experimental value of M_{η_c} remains ambiguous: the PDG [2] average is based on a fit to measurements with poor internal consistency [6–8], the confidence level of the fit is only 0.001. A recent measurement from E760 [6] disagrees with the value reported by the DM2 group [7] by almost four standard deviations. Additional measurements may help clarify the situation.

The data were taken with the BES detector at the BEPC storage ring at a center-of-mass energy corresponding to $m_{\psi(2S)}$. The data sample corresponds to a total of $(3.79 \pm 0.31) \times 10^6$ $\psi(2S)$ decays, as determined from the observed number of inclusive $\psi(2S) \to \pi^+\pi^- J/\psi$ decays [9].

II. THE BES DETECTOR

BES is a conventional solenoidal magnet detector that is described in detail in Ref. [10]. A four-layer central drift chamber (CDC) surrounding the beampipe provides trigger information. A forty-layer cylindrical main drift chamber (MDC), located radially outside the CDC, provides trajectory and energy loss (dE/dx) information for charged tracks over 85% of the total solid angle. The momentum resolution is $\sigma_p/p = 0.017\sqrt{1+p^2}$ (p in GeV/c), and the dE/dx resolution for hadron tracks is $\sim 11\%$. An array of 48 scintillation counters surrounding the MDC measures the time-of-flight (TOF) of charged tracks with a resolution of ~ 450 ps for hadrons. Radially outside of the TOF system is a 12 radiation length thick, lead-gas barrel shower counter (BSC) operating in the limited streamer mode. This device covers $\sim 80\%$ of the total solid angle and measures the energies of electrons and photons over with an energy resolution of $\sigma_E/E = 22\%/\sqrt{E}$ (E in GeV). Outside of the solenoid magnet coil, which provides a 0.4 Tesla magnetic field over the tracking volume, is an iron flux return that is instrumented with three double layers of counters that identify muons of momentum greater than 0.5 GeV/c.

III. MONTE CARLO

We use Monte Carlo simulated events to determine the detection efficiency (ε) and the mass resolution (σ_{res}) for each channel analyzed. The Monte Carlo program (MC) generates events of the type $\psi(2S) \to \gamma\chi_{cJ}$ under the assumption that these processes are pure $E1$ transitions [3,11]: the photon polar angle distributions are $1+\cos^2\theta \;\; (\chi_{c0})$, $1-\frac{1}{3}\cos^2\theta \;\; (\chi_{c1})$ and $1+\frac{1}{13}\cos^2\theta \;\; (\chi_{c2})$. Multihadronic χ_{cJ} decays are simulated using phase space distributions. For each channel, either 10000 or 5000 events are generated, depending on the numbers of events for the corresponding mode that are observed in the data sample.

IV. EVENT SELECTION

A. Photon Identification

A neutral cluster is considered to be a photon candidate when the angle in the xy plane between the nearest charged track and the cluster is greater than 15°, the first hit is in the beginning 6 radiation lengths, and the difference between the angle of the cluster development direction in the BSC and the photon emission direction is less than 37°. When these selection criteria are applied to kinematically selected samples of $\psi(2S) \to \pi^+\pi^-\pi^+\pi^-$ and $\psi(2S) \to \pi^+\pi^-K^+K^-$ events, fewer than 20% of the events have γ candidates, which indicates that the fake-photon rejection ability is high (see Fig. 1). After identification, the number of photon candidates in an event is limited to four or less. The photon candidate with the largest energy deposit in the BSC is considered to be the photon radiated from $\psi(2S)$ and used in a four-constraint kinematic fit to the hypothesis

$\psi(2S) \to \gamma +$ charged tracks assignment.

B. Charged Particle Identification

Each charged track is required to be well fit to a three-dimensional helix and be in the polar angle region $|\cos\theta_{MDC}| < 0.8$. For each track, the TOF and dE/dx measurements are used to calculate χ^2 values and the corresponding confidence levels to the hypotheses that the particle is a pion, kaon and proton $(Prob_\pi, Prob_K, Prob_p)$. The reliability of the confidence level assignments is verified using a sample of $\psi(2S) \to \pi^+\pi^- J/\psi$, $J/\psi \to \rho\pi$ and $J/\psi \to K^+K^-$ events, where the particle identification confidence levels $(ProbID)$ of the tracks in different momentum ranges are found to be distributed uniformly between zero and one as expected [12]. Typically the $ProbID$ value of each track for a given decay hypothesis is required to be greater than 1% in our analysis.

C. Event Selection Criteria

For all decay channels, the candidate events are required to satisfy the following selection criteria:

1. The number of charged tracks is required to be four or six with net charge zero.

2. The maximum number of neutral clusters in one event is eight, and the number of photon candidates remaining after the application of the photon selection is required to be four or less.

3. The total momentum of the lowest momentum π^+ and π^- tracks is required to be greater than 550 MeV; this removes contamination from $\psi(2S) \to \pi^+\pi^- J/\psi$ events.

4. The χ^2 probability for a four-constraint kinematic fit to the decay hypothesis is Prob4C > 0.01.

5. The particle identification assignment of each charged track is $ProbID > 0.01$.

1. $\gamma\pi^+\pi^-\pi^+\pi^-$ and $\gamma\pi^+\pi^-K^+K^-$

A combined probability of the four-constraint kinematic fit and particle identification information is used to separate $\gamma\pi^+\pi^-\pi^+\pi^-$ and the different particle assignments for the $\gamma\pi^+\pi^-K^+K^-$ final states. This combined probability, $Prob_{all}$, is defined as

$$Prob_{all} = Prob(\chi^2_{\mathrm{all}}, ndf_{\mathrm{all}}),$$

where χ^2_{all} is the sum of the χ^2 values from the four-constraint kinematic fit and those from each of the four particle identification assignments, and ndf_{all} is the corresponding total number of degrees of the freedom used in the χ^2 determinations. The particle assignment with largest $Prob_{all}$ is regarded as the correct assumption and further cuts on the kinematic fit probability and particle identification probability are imposed.

Figure 2 shows a scatterplot of $\pi^+\pi^-$ vs $\pi^+\pi^-$ invariant masses for events with a $\pi^+\pi^-\pi^+\pi^-$ mass between 3.2 and 3.6 GeV. The cluster of events in the lower left-hand corner indicates the presence of a $K^0_sK^0_s$ signal. A fit of a Gaussian function to the $\pi^+\pi^-$ mass distribution gives a peak mass at 499.3 ± 1.2 MeV and a width $\sigma = 11.8\pm1.0$ MeV that is consistent with the MC expectation for the mass resolution. We select $\gamma K^0_sK^0_s$ candidates by requiring the mass of both $\pi^+\pi^-$ combinations in the event to be within $\pm2\sigma$ of the nominal K^0_s mass.

The invariant mass distributions for the $\pi^+\pi^-\pi^+\pi^-$, $\pi^+\pi^-K^+K^-$ and $K^0_sK^0_s$ events that survive all the selection requirements are shown in Figs. 3, 4 and 5. There are peaks corresponding to the χ_{cJ} states in each of the plots. The high mass peaks in Figs. 3 and 4 correspond to the $\psi(2S)$ decays to all charged tracks final states but kinematically fitted with a fake photon.

We fit the $\pi^+\pi^-\pi^+\pi^-$, $\pi^+\pi^-K^+K^-$ or $K^0_sK^0_s$ invariant mass distribution between 3.20 and 3.65 GeV with three Breit-Wigner resonances convoluted with Gaussian mass resolution functions and a linear background shape using an unbinned maximum likelihood method. In the fit, the mass resolutions are fixed to their MC-determined values and the widths of the χ_{c1} and χ_{c2} are fixed to the PDG average values of of 0.88 and 2.00 MeV [2], respectively. The results of the fit are listed in Table I and shown in Figs. 3, 4 and 5. Table I also lists the MC-determined efficiencies and mass resolutions.

2. $\gamma\pi^+\pi^-p\bar{p}$

If one of the four tracks is identified as a proton or antiproton, the event is assumed to be $\gamma\pi^+\pi^-p\bar{p}$. We assign probabilities to the remaining particle assignment using the same technique that was used for $\pi^+\pi^-K^+K^-$ decays; the combination with the highest probability is selected.

The $\pi^+\pi^-p\bar{p}$ invariant mass distribution for the selected events is shown in Fig. 6. Here clear signals for all three χ_{cJ} states are apparent. We fit the mass spectrum using the same method described in the previous section; the results are listed in Table II and shown as the smooth curve in Fig. 6.

3. $\gamma K^+K^-K^+K^-$

For the case where all the tracks are kaons, the contamination from $\pi^+\pi^-J/\psi$ is not an important background and the requirement on total momentum of the lowest momentum π^+ and π^- tracks, which is aimed at removing these events, is not used. The $K^+K^-K^+K^-$ invariant mass distribution is shown in Fig. 7.

Figure 8 shows a scatterplot of K^+K^- vs K^+K^- invariant masses for the events with $K^+K^-K^+K^-$ mass between 3.2 and 3.6 GeV. The concentration of events in the lower left-hand corner of the plot indicates the presence of $\phi\phi$ final states. A fit to the K^+K^- mass distribution with a Gaussian function gives a peak mass of 1021.9 ± 0.8 MeV and a width $\sigma = 5.3 \pm 0.6$ MeV, consistent with MC expectations. Events where the mass of two K^+K^- combinations to be in the range $0.99 < M_{K^+K^-} < 1.05$ GeV are identified as $\gamma\phi\phi$ candidates. The $\phi\phi$ mass distribution for these events is shown in Fig. 9, where there are clear signals for the χ_{c0} and χ_{c2}.

The $K^+K^-K^+K^-$ mass and $\phi\phi$ mass plots are fitted with three Breit-Wigner resonances and two Breit-Wigner resonances, respectively, as described previously. The results of the fit are listed in Table III and are shown as smooth curves in Figs. 7 and 9.

Because of the large fraction of $\phi\phi$ intermediate events observed in the $K^+K^-K^+K^-$ mode and the significant difference between the detection efficiency for phase-space events and those coming from $\phi\phi$ decays, the detection efficiency for the χ_{c0} and $\chi_{c2} \rightarrow K^+K^-K^+K^-$ channels is a weighted average of the phase space and $\phi\phi$ efficiency. The detection efficiencies and mass resolutions are listed in Table III.

4. $\gamma K_s^0 K^+\pi^- + c.c.$

The $\chi_{cJ} \rightarrow K_s^0 K^+\pi^- + c.c.$ decay channels have serious potential backgrounds from $\gamma\pi^+\pi^-\pi^+\pi^-$ (including $\gamma K_s^0 K_s^0$) and $\gamma\pi^+\pi^-K^+K^-$ final states. To eliminate these backgrounds, we exploit the feature that there is one and only one K_s^0 with a secondary vertex in real $K_s^0 K^+\pi^- + c.c.$ events.

In each event, we determine $NKSHORT$, the number of two charged track combinations with net charge zero and effective mass within ± 200 MeV of M_{K^0}, when the tracks are assigned a pion mass. The combination with mass closest to M_{K^0} is considered to be a K_s^0 candidate. The K_s^0 vertex is defined as the point of closest approach of these two tracks; the primary vertex is defined as the point of closest approach of the other two charged tracks in the event. Two parameters are used to identify the K_s^0: the distance between primary vertex and secondary vertex in the xy plane, L_{xy}, and the cosine of the angle between the K_s^0 momentum vector and its vertex direction $CSKS$, which is expected to be very near unity for a real K_s^0 event.

Candidate $\gamma K_s^0 K^+\pi^- + c.c.$ events are selected by requiring the mass of the K_s^0 candidate determined from the track four-vectors returned by the 4C-fit to be within $\pm 2\sigma$ (i.e. $\pm$ 28 MeV) of the nominal K^0 mass, $NKSHORT = 1$, $L_{xy} > 5$ mm, and $CSKS > 0.98$. In the invariant mass distribution of the selected events, shown in Fig. 10, only a χ_{c1} signal is prominent. The MC simulation indicates that the numbers of events in the the χ_{c0} and χ_{c2} mass region are consistent with residual backgrounds from $\gamma\pi^+\pi^-\pi^+\pi^-$, $\gamma K_s^0 K_s^0$ and $\gamma\pi^+\pi^- K^+ K^-$ final states. We set upper limits on the branching fractions of χ_{c0} and χ_{c2}.

The $K_s^0 K^+\pi^- + c.c.$ invariant mass distribution between 3.20 and 3.65 GeV are fitted with the procedure described above. The mass resolutions are fixed at their MC-determined values, the width of the χ_{c0} is fixed at the recent BES value of 14.3 MeV [5] and those of the χ_{c1} and χ_{c2} at their PDG values [2]. The mass of the three χ_c states are also fixed at their PDG [2] values. The fit results are listed in Table IV and are shown as a smooth curve in Fig. 10.

5. $\gamma 3(\pi^+\pi^-)$

After the selections based on the kinematic fit and particle ID, the main background to the $\chi_{cJ} \to 3(\pi^+\pi^-)$ decays comes from the decay chain $\psi(2S) \to \pi^+\pi^- J/\psi, J/\psi \to \gamma\pi^+\pi^-\pi^+\pi^-$. The requirement on the total momentum of the lowest momentum π^+ and π^- tracks removes one third of the MC-simulated events while rejecting almost all the $\pi^+\pi^- J/\psi$ background.

The $3(\pi^+\pi^-)$ invariant mass distribution for the selected events is shown in Fig. 11, where prominent signals for all three χ_{cJ} states can be seen. The smooth curve in the figure is the result of the fitting procedure described above. The results of the fit and the MC-determined efficiencies and resolutions are listed in Table V.

V. BRANCHING FRACTION DETERMINATION

We determine branching fractions from the relation

$$\mathcal{B}(\chi_{cJ} \to X) = \frac{n^{obs}/\varepsilon(\chi_{cJ} \to X)}{N_{\psi(2S)}\mathcal{B}(\psi(2S) \to \gamma\chi_{cJ})},$$

where the values for $\mathcal{B}(\psi(2S) \to \gamma\chi_{cJ})$ are taken from the PDG tables [2]. For the $K_s^0 K_s^0$ [$\phi\phi$] channel, a factor of $\mathcal{B}(K_s^0 \to \pi^+\pi^-)^2$ [$\mathcal{B}(\phi \to K^+K^-)^2$] is included in the denominator.

A. Systematic errors

Systematic errors common to all modes include the uncertainties in the total number of $\psi(2S)$ events (8.2%) and the $\psi(2S) \to \gamma\chi_{cJ}$ branching fractions (8.6%, 9.2% and 10.3% for χ_{c0}, χ_{c1} and χ_{c2}, respectively).

Other sources of systematic errors were considered. The variation of our results for different choices of the selection criteria range from 10% for high statistics channels to 25% for those with low statistics. The systematic errors due to the statistical precision of the MC event samples range from 2% to 5% depending on the detection efficiencies of the channels. Changes in the detection efficiency when the phase space event generator is replaced by one using possible intermediate resonant states indicate that the systematic error on the efficiency due to the unknown dynamics of the decay processes is 15%. The variation of the numbers of observed events due to shifts of the mass resolutions and the total widths of the χ_{cJ} states is 7%; that coming from changes in the shape used for the background function is less than 5%.

The total systematic error is taken as the quadrature sum the individual errors and ranges from 25% to 35%, depending on the channel.

B. Branching fraction results

The branching fraction results are listed in Table VI, where all BES results for χ_{cJ} branching fractions are given, including those for the two-charged track modes reported in Ref. [5]. In each case, the first error listed is statistical and the second is systematic. For comparison, we also provide the previous world averages for those channels when they exist [2].

Our branching fractions for $\chi_{c1} \to K_s^0 K^+ \pi^- + c.c.$, $\chi_{c0} \to K_s^0 K_s^0$, $\chi_{c2} \to K_s^0 K_s^0$, $\chi_{c0} \to \phi\phi$, $\chi_{c2} \to \phi\phi$ and $\chi_{cJ} \to K^+K^-K^+K^-$ (J=0,1,2) are the first reported measurements for these decays. The results for χ_{c0} and $\chi_{c2} \to K_s^0 K_s^0$ are in agreement with the isospin prediction of the χ_{cJ} decays compared with the corresponding K^+K^- branching ratios.

For the other decay modes, signals with large statistics are observed and the corresponding branching fractions are determined with precisions that are significantly better than those of existing measurements. Note that our results are consistently lower than the previous measurements, sometimes by as much as a factor of two or more. We can find no obvious explanation for these discrepancies.

VI. DETERMINATION OF $M_{\chi_{C0}}$ AND M_{η_C}

We determine $M_{\chi_{c0}}$ by fitting the combined invariant mass distribution of all of the channels discussed above to three resolution-broadened Breit-Wigner functions with the resolution fixed at the value of 13.8 MeV, which is determined from fits to the χ_{c1} and χ_{c2}, and the total widths of the χ_{c1} and χ_{c2} fixed at the PDG values [2]. The masses of all three χ_{cJ} states and the total width of the χ_{c0} are left as free parameters. The results of the fit for $M_{\chi_{c1}}$ and $M_{\chi_{c2}}$ agree with the PDG values within errors. The fit value for $M_{\chi_{c0}}$ is 3414.1 ± 0.6 MeV, where the error is statistical. The fit gives a total width for the χ_{c0} that is in good agreement with the recently reported BES result [5].

Figure 12 shows the combined invariant mass distribution for the $\pi^+\pi^-\pi^+\pi^-$, $\pi^+\pi^-K^+K^-$, $K^+K^-K^+K^-$, and $K^0_sK^+\pi^- + c.c.$ channels in the region of the η_c, where an η_c signal is evident. Superimposed on the plot is a fit to the spectrum using a resolution-smeared Breit-Wigner line shape with a mass that is allowed to vary, a total width fixed at the PDG value of $\Gamma_{\eta_c} = 13.2$ MeV [2], and a fourth-order polynomial background function. The fit gives a total of 63.5 ± 14.4 events in the peak and has a $\chi^2/dof = 97.4/92$, which corresponds to a confidence level of 27.9%. The mass value from the fit is $M_{\chi_{\eta_c}} = 2975.8 \pm 3.9$ MeV, where the error is statistical. (A fit with only the background function and no η_c has a confidence level of 0.8%.)

The systematic error on the mass determination includes a possible uncertainty in the overall mass scale (± 0.8 MeV), which is determined from the rms average of the differences between the fitted values for $M_{\chi_{c1}}$ and $M_{\chi_{c2}}$ and their PDG values. The systematic errors associated with uncertainties is the particle's total widths and the experimental resolutions (± 0.95 MeV for M_{η_c} and less than 0.2 MeV for $M_{\chi_{c0}}$) are added in quadrature. The resulting masses and errors are:

$$M_{\chi_{c0}} = 3414.1 \pm 0.6(\text{stat}) \pm 0.8(\text{sys}) \quad \text{MeV},$$

and

$$M_{\eta_c} = 2975.8 \pm 3.9(\text{stat}) \pm 1.2(\text{sys}) \quad \text{MeV}.$$

The precision of our $M_{\chi_{c0}}$ measurement represents a substantial improvement on the existing PDG value of 3417.3 ± 2.8 MeV [2]. Our result for M_{η_c} agrees with the DM2 group's value of 2974.4 ± 1.9 MeV [7] and is 2.4 standard deviations below the E760 group's result of $2988.3^{+3.3}_{-3.1}$ MeV [6].

VII. SUMMARY

Events of the type $\psi(2S) \to \gamma\chi_{cJ}$ in a 3.79×10^6 $\psi(2S)$ event sample are used to determine branching fractions for χ_{cJ} decays to four and six charged particle final states. Our results for $K_s^0K^+\pi^- + c.c.$, $K_s^0K_s^0$, $\phi\phi$, and $K^+K^-K^+K^-$ are the first measurements for these decays. The branching fractions for $\chi_{cJ} \to \pi^+\pi^-\pi^+\pi^-$, $\pi^+\pi^-K^+K^-$, $\pi^+\pi^-p\bar{p}$, and $3(\pi^+\pi^-)$ final states are measured with better precision and found to be consistently lower than previous measurements. We use the same data sample to determine $M_{\chi_{c0}}$ and M_{η_c}. Our result for M_{η_c} agrees with the DM2 result [7] and is below that of E760 [6].

ACKNOWLEDGMENTS

We thank the staffs of the BEPC Accelerator and the Computing Center at the Institute of High Energy Physics, Beijing, for their outstanding scientific efforts. This project was partly supported by China Postdoctoral Science Foundation. The work of the BES Collaboration was supported in part by the National Natural Science Foundation of China under Contract No. 19290400 and the Chinese Academy of Sciences under contract No. KJ85 (IHEP), and by the Department of Energy under Contract Nos. DE-FG03-92ER40701 (Caltech), DE-FG03-93ER40788 (Colorado State University), DE-AC03-76SF00515 (SLAC), DE-FG03-91ER40679 (UC Irvine), DE-FG03-94ER40833 (U Hawaii), DE-FG03-95ER40925 (UT Dallas).

REFERENCES

† Deceased.

[1] W. Braunschweig *et al.* (DASP Collab.), Phys. Lett. **B57**, 407 (1975); G. J. Feldman *et al.* (Mark1 Collab.), Phys. Rev. Lett. **35**, 821 (1975).

[2] C. Caso *et al.* (Particle Data Group), Eur. Phys. J. **C3**, 1 (1998) and references therein.

[3] W. Tanenbaum *et al.* (Mark1 Collab.), Phys. Rev. **D17**, 1731 (1978).

[4] T. Armstrong *et al.* (E760 Collaboration), Phys. Rev. Lett. **68**, 1468 (1992).

[5] J. Z. Bai *et al.* (BES Collab.), Phys. Rev. Lett. **81**, 3091 (1998).

[6] T. A. Armstrong *et al.* (E760 Collab.), Phys. Rev. **D52**, 4839 (1995).

[7] D. Bisello *et al.*, (DM2 Collab.), Nucl. Phys. **B350**, 1 (1991).

[8] R. M. Baltrusaitis *et al.* (Mark3 Collab.), Phys. Rev. **D33**, 629 (1986); J. E. Gaiser *et al.* (Crystal Ball Collab.), Phys. Rev. **D34**, 711 (1986); C. Bagelin *et al.*, Phys. Lett. **B231**, 557 (1989); and Z. Bai *et al.* (Mark3 Collab.), Phys. Rev. Lett. **65**, 1309 (1990).

[9] J. Z. Bai *et al.* (BES Collab.), Phys. Rev. **D58**, 092006 (1998).

[10] J. Z. Bai *et al.* (BES Collab.), Nucl. Instrum. Methods Phys. Res., Sect. **A344**, 319 (1994).

[11] G. Karl, S. Meshkov and J. L. Rosner, Phys.Rev., **D13**, 1203 (1976); M. Oreglia *et al.* (Crystal Ball Collab.), Phys. Rev. **D25**, 2259 (1982).

[12] Using the $\psi(2S) \to \pi^+\pi^- K^+K^-$ events sample and the particle identification procedures described in the text, we determine the branching fraction $\mathcal{B}(J/\psi \to K^+K^-) = (2.35 \pm 0.34 \pm 0.44) \times 10^{-4}$, which is in good agreement with the world average [2].

FIGURES

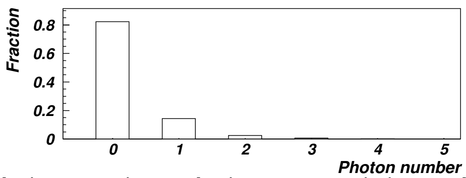

FIG. 1. The distribution of the number of photon candidates found in $\psi(2S) \to \pi^+\pi^-\pi^+\pi^-$ and $\psi(2S) \to \pi^+\pi^- K^+K^-$ events.

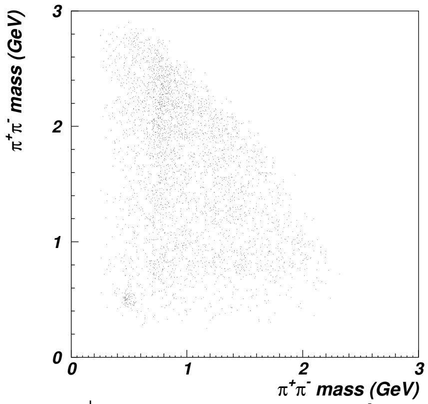

FIG. 2. A scatterplot of $\pi^+\pi^-$ vs $\pi^+\pi^-$ invariant masses for selected $\gamma\pi^+\pi^-\pi^+\pi^-$ events (two entries per event).

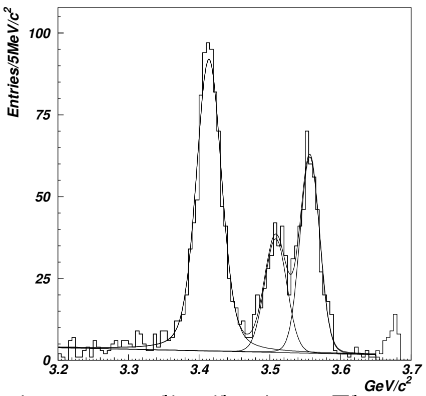

FIG. 3. The $\pi^+\pi^-\pi^+\pi^-$ invariant mass distribution. The smooth curve is the result of a fit described in the text.

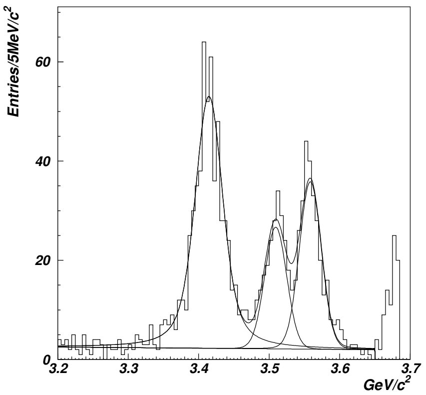

FIG. 4. The $\pi^+\pi^-K^+K^-$ invariant mass distribution. The smooth curve is the result of a fit described in the text.

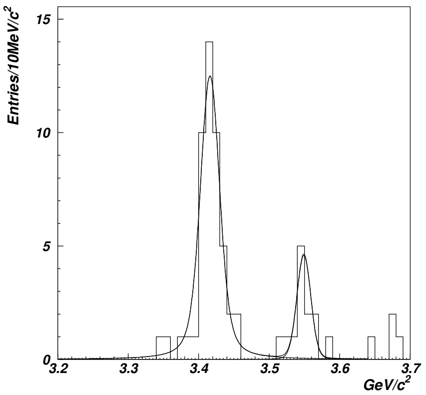

FIG. 5. The $K_s^0 K_s^0$ invariant mass distribution. The smooth curve is the result of a fit described in the text.

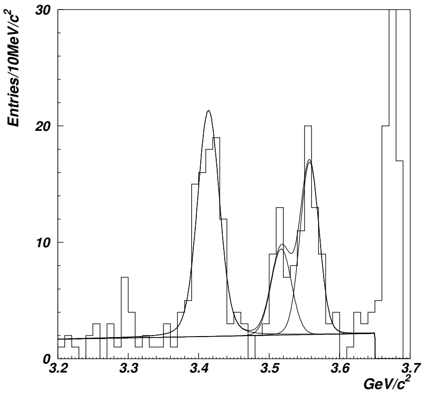

FIG. 6. The $\pi^+\pi^-p\bar{p}$ invariant mass distribution. The smooth curve is the result of a fit described in the text.

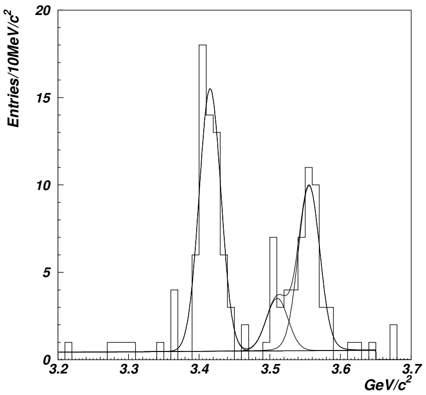

FIG. 7. The $K^+K^-K^+K^-$ invariant mass distribution. The smooth curve is the result of a fit described in the text.

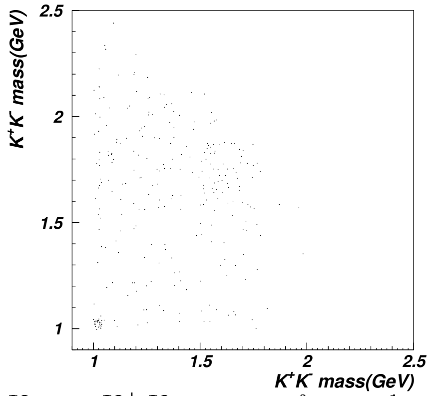

FIG. 8. A scatterplot of K^+K^- vs K^+K^- masses from selected $\gamma K^+K^-K^+K^-$ events (two entries per event).

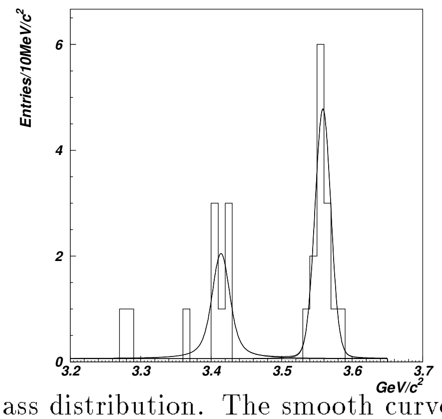

FIG. 9. The $\phi\phi$ invariant mass distribution. The smooth curve is the result of a fit described in the text.

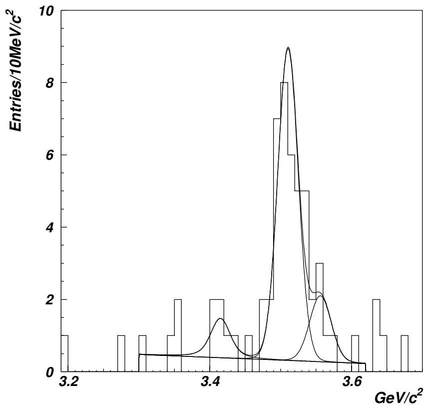

FIG. 10. The $K_s^0K^+\pi^- + c.c.$ invariant mass distribution. The smooth curve is the result of a fit described in the text.

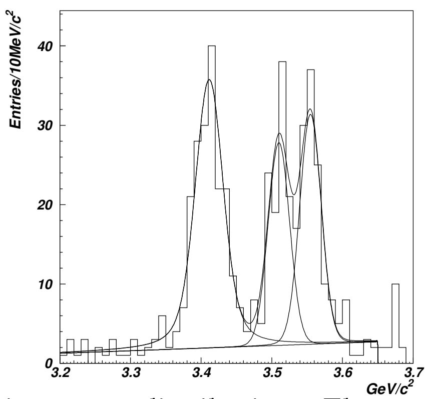

FIG. 11. The $3(\pi^+\pi^-)$ invariant mass distribution. The smooth curve is the result of a fit described in the text.

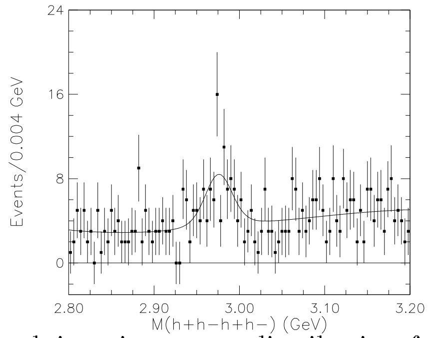

FIG. 12. The four charged track invariant mass distribution for selected events in the η_c mass region. The superimposed curve is the result of fit described in the text.

TABLES

TABLE I. Fit results for $\chi_{cJ} \to \pi^+\pi^-\pi^+\pi^-, \pi^+\pi^- K^+K^-$ and $K^0_s K^0_s$ decays.

Channel	n^{obs}	ε (%)	σ_{res} (MeV)
$\chi_{c0} \to \pi^+\pi^-\pi^+\pi^-$	874 ± 30	16.06	15.1
$\chi_{c1} \to \pi^+\pi^-\pi^+\pi^-$	277 ± 19	17.06	15.6
$\chi_{c2} \to \pi^+\pi^-\pi^+\pi^-$	425 ± 21	15.09	13.4
$\chi_{c0} \to K^0_s K^0_s$	49.3 ± 7.0	15.16	10.9
$\chi_{c2} \to K^0_s K^0_s$	11.7 ± 3.2	13.92	9.4
$\chi_{c0} \to \pi^+\pi^- K^+K^-$	587 ± 27	11.32	14.4
$\chi_{c1} \to \pi^+\pi^- K^+K^-$	192 ± 16	12.91	15.3
$\chi_{c2} \to \pi^+\pi^- K^+K^-$	267 ± 18	11.42	15.1

TABLE II. Fit results for $\chi_{cJ} \to \pi^+\pi^- p\bar{p}$ decays.

Channel	n^{obs}	ε (%)	σ_{res} (MeV)
χ_{c0}	81 ± 10	14.62	13.9
χ_{c1}	27.1 ± 6.9	16.72	14.3
χ_{c2}	50.9 ± 8.1	13.98	13.0

TABLE III. Fit results for $\chi_{cJ} \to K^+K^-K^+K^-$ and $\phi\phi$ decays.

Channel	n^{obs}	ε (%) (PS/$\phi\phi$)	σ_{res} (MeV)
$\chi_{c0} \to K^+K^-K^+K^-$	57.8 ± 6.9	7.38/10.06	15.4
$\chi_{c1} \to K^+K^-K^+K^-$	11.7 ± 4.2	8.52/no	15.2
$\chi_{c2} \to K^+K^-K^+K^-$	36.6 ± 5.9	7.64/9.76	14.7
$\chi_{c0} \to \phi\phi$	7.6 ± 2.8	9.78	8.9
$\chi_{c2} \to \phi\phi$	13.6 ± 3.7	9.54	10.8

TABLE IV. Fit results for $\chi_{cJ} \to K_s^0 K^+\pi^- + c.c.$ decays. The upper limits are 90% confidence level values.

Channel	n^{obs}	ε (%)	σ_{res} (MeV)
χ_{c0}	< 8.5	4.94	10.3
χ_{c1}	31.4 ± 5.6	5.64	14.2
χ_{c2}	< 10.6	4.93	14.7

TABLE V. Fit results for $\chi_{cJ} \to 3(\pi^+\pi^-)$ decays.

Channel	n^{obs}	ε (%)	σ_{res} (MeV)
χ_{c0}	191 ± 16	4.62	15.8
χ_{c1}	98 ± 12	5.20	15.0
χ_{c2}	112 ± 12	4.23	14.7

TABLE VI. The χ_{cJ} hadronic decay branching fractions, determined using $\mathcal{B}(\psi(2S) \to \gamma\chi_{c0}) = (9.3 \pm 0.8)\%$, $\mathcal{B}(\psi(2S) \to \gamma\chi_{c1}) = (8.7 \pm 0.8)\%$ and $\mathcal{B}(\psi(2S) \to \gamma\chi_{c2}) = (7.8 \pm 0.8)\%$.

Channel	n^{obs}	Branching Ratio	World Average [2]
$\chi_{c0} \to \pi^+\pi^-$	720 ± 32	$(4.68 \pm 0.26 \pm 0.65) \times 10^{-3}$	$(7.5 \pm 2.1) \times 10^{-3}$
$\chi_{c2} \to \pi^+\pi^-$	185 ± 16	$(1.49 \pm 0.14 \pm 0.22) \times 10^{-3}$	$(1.9 \pm 1.0) \times 10^{-3}$
$\chi_{c0} \to K^+K^-$	774 ± 38	$(5.68 \pm 0.35 \pm 0.85) \times 10^{-3}$	$(7.1 \pm 2.4) \times 10^{-3}$
$\chi_{c2} \to K^+K^-$	115 ± 13	$(0.79 \pm 0.14 \pm 0.13) \times 10^{-3}$	$(1.5 \pm 1.1) \times 10^{-3}$
$\chi_{c0} \to p\bar{p}$	15.2 ± 4.1	$(15.9 \pm 4.3 \pm 5.3) \times 10^{-5}$	$< 9.0 \times 10^{-4}$
$\chi_{c1} \to p\bar{p}$	4.2 ± 2.2	$(4.2 \pm 2.2 \pm 2.8) \times 10^{-5}$	$(8.6 \pm 1.2) \times 10^{-5}$
$\chi_{c2} \to p\bar{p}$	4.7 ± 2.5	$(5.8 \pm 3.1 \pm 3.2) \times 10^{-5}$	$(10.0 \pm 1.0) \times 10^{-5}$
$\chi_{c0} \to \pi^+\pi^-\pi^+\pi^-$	874 ± 30	$(15.4 \pm 0.5 \pm 3.7) \times 10^{-3}$	$(3.7 \pm 0.7) \times 10^{-2}$
$\chi_{c1} \to \pi^+\pi^-\pi^+\pi^-$	277 ± 19	$(4.9 \pm 0.4 \pm 1.2) \times 10^{-3}$	$(1.6 \pm 0.5) \times 10^{-2}$
$\chi_{c2} \to \pi^+\pi^-\pi^+\pi^-$	425 ± 21	$(9.6 \pm 0.5 \pm 2.4) \times 10^{-3}$	$(2.2 \pm 0.5) \times 10^{-2}$
$\chi_{c0} \to K^0_sK^0_s$	49.3 ± 7.0	$(1.96 \pm 0.28 \pm 0.52) \times 10^{-3}$	
$\chi_{c2} \to K^0_sK^0_s$	11.7 ± 3.2	$(0.61 \pm 0.17 \pm 0.16) \times 10^{-3}$	
$\chi_{c0} \to \pi^+\pi^-K^+K^-$	587 ± 27	$(14.7 \pm 0.7 \pm 3.8) \times 10^{-3}$	$(3.0 \pm 0.7) \times 10^{-2}$
$\chi_{c1} \to \pi^+\pi^-K^+K^-$	192 ± 16	$(4.5 \pm 0.4 \pm 1.1) \times 10^{-3}$	$(9 \pm 4) \times 10^{-3}$
$\chi_{c2} \to \pi^+\pi^-K^+K^-$	267 ± 18	$(7.9 \pm 0.6 \pm 2.1) \times 10^{-3}$	$(1.9 \pm 0.5) \times 10^{-2}$
$\chi_{c0} \to \pi^+\pi^-p\bar{p}$	81 ± 11	$(1.57 \pm 0.21 \pm 0.54) \times 10^{-3}$	$(5.0 \pm 2.0) \times 10^{-3}$
$\chi_{c1} \to \pi^+\pi^-p\bar{p}$	27.1 ± 6.9	$(0.49 \pm 0.13 \pm 0.17) \times 10^{-3}$	$(1.4 \pm 0.9) \times 10^{-3}$
$\chi_{c2} \to \pi^+\pi^-p\bar{p}$	50.9 ± 8.1	$(1.23 \pm 0.20 \pm 0.35) \times 10^{-3}$	$(3.3 \pm 1.3) \times 10^{-3}$
$\chi_{c0} \to K^+K^-K^+K^-$	57.8 ± 6.9	$(2.14 \pm 0.26 \pm 0.40) \times 10^{-3}$	
$\chi_{c1} \to K^+K^-K^+K^-$	11.7 ± 4.2	$(0.42 \pm 0.15 \pm 0.12) \times 10^{-3}$	
$\chi_{c2} \to K^+K^-K^+K^-$	36.6 ± 5.9	$(1.48 \pm 0.26 \pm 0.32) \times 10^{-3}$	
$\chi_{c0} \to \phi\phi$	7.6 ± 2.8	$(0.92 \pm 0.34 \pm 0.38) \times 10^{-3}$	

$\chi_{c2} \to \phi\phi$	13.6 ± 3.7	$(2.00 \pm 0.55 \pm 0.61) \times 10^{-3}$	
$\chi_{c0} \to K_s^0 K^+ \pi^- + c.c.$	< 8.5	$< 0.71 \times 10^{-3}$	
$\chi_{c1} \to K_s^0 K^+ \pi^- + c.c.$	31.4 ± 5.6	$(2.46 \pm 0.44 \pm 0.65) \times 10^{-3}$	
$\chi_{c2} \to K_s^0 K^+ \pi^- + c.c.$	< 10.6	$< 1.06 \times 10^{-3}$	
$\chi_{c0} \to 3(\pi^+\pi^-)$	191 ± 16	$(11.7 \pm 1.0 \pm 2.3) \times 10^{-3}$	$(1.5 \pm 0.5) \times 10^{-2}$
$\chi_{c1} \to 3(\pi^+\pi^-)$	98 ± 12	$(5.8 \pm 0.7 \pm 1.2) \times 10^{-3}$	$(2.2 \pm 0.8) \times 10^{-2}$
$\chi_{c2} \to 3(\pi^+\pi^-)$	112 ± 12	$(9.0 \pm 1.0 \pm 2.0) \times 10^{-3}$	$(1.2 \pm 0.8) \times 10^{-2}$